# Accepted Manuscript

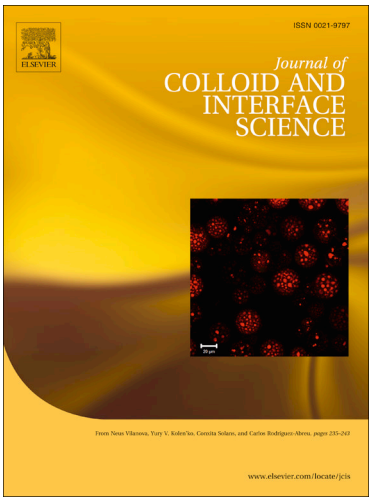


Fully nozzle-jet printed non-enzymatic electrode for biosensing application

Kiesar Sideeq Bhat, Rafiq Ahmad, Jin-Young Yoo, Yoon-Bong Hahn

PII: S0021-9797(17)31259-6
DOI: https://doi.org/10.1016/j.jcis.2017.10.088
Reference: YJCIS 22958

To appear in: *Journal of Colloid and Interface Science*

Received Date: 19 September 2017
Revised Date: 19 October 2017
Accepted Date: 23 October 2017

Please cite this article as: K.S. Bhat, R. Ahmad, J-Y. Yoo, Y-B. Hahn, Fully nozzle-jet printed non-enzymatic electrode for biosensing application, *Journal of Colloid and Interface Science* (2017), doi: https://doi.org/10.1016/j.jcis.2017.10.088

# Fully nozzle-jet printed non-enzymatic electrode for biosensing application

Kiesar Sideeq Bhat[1], Rafiq Ahmad[1], Jin-Young Yoo and Yoon-Bong Hahn*

*School of Semiconductor and Chemical Engineering, Nanomaterials Processing Research Center, Chonbuk National University, 567 Baekjedaero, Deokjin-gu, Jeonju-si, Jeollabuk-do, 54896, Republic of Korea.*

* **Corresponding author**. Tel.: +82-63-2702439; Fax: +82-63-2702306

E-mail: ybhahn@chonbuk.ac.kr (Y. B. Hahn)

[1]These authors contributed equally to this work.

**Abstract**

The progress in developing the electrochemical sensors for biomolecule detection requires a facile device fabrication method. Herein, we report printing of silver (Ag) precursor and copper oxide nanoparticles (CuO NPs) inks by nozzle-jet technique to fabricate non-enzymatic glucose biosensor on flexible polyethylene terephthalate (PET) substrate. The fully printed CuO NPs/Ag/PET electrodes were characterized using electrochemical techniques for non-enzymatic biosensing of glucose. The fully printed non-enzymatic biosensor exhibited a high sensitivity (1424.2 μA $mM^{-1}cm^{-2}$), linear range from 0.1 to 15 mM, low detection limit (0.3 μM; S/N = 3) and fast response time of ~2s under a working potential of +0.6V. Additionally, printed electrodes demonstrated an excellent long term stability, high reproducibility, good selectivity and high accuracy during glucose concentration measurements in human blood and serum samples. These results indicate that the electrode fabrication using nozzle-jet printing can be regarded as a potential technique for the future development of high performance and low cost bio/chemical sensor devices.

**Keywords**: nozzle-jet printing; non-enzymatic; glucose biosensor; long term stability

## 1. Introduction

Glucose detection offers a prominent technical importance to scientists for clinical diagnostics of diabetes, analytical applications and food industry [1-5]. Generally, in diabetic patients and healthy people the blood glucose levels are in the range of 1.1-20.8 and 3.6-7.5 mM, respectively. The electrochemical sensing technique, being a precise technology, can measure glucose with high accuracy for clinical purposes. However, enzymatic biosensors have serious drawback of week stability due to the intrinsic nature of enzymes, critical operating conditions, complicated immobilization procedures, and high cost of enzymes [6, 7]. Therefore, several methods have been utilized to encompass and measure glucose with high sensitivity [7, 8, 9]. However, some problems like low sensitivity and poor selectivity are associated with most of the non-enzymatic sensors which can be imputed to the adsorption of intermediates [10, 11]. Hence, it is essential to investigate and develop a highly sensitivity, reproducible, cost effective and stable non-enzymatic glucose biosensor in order to achieve promising clinical measurements.

Copper oxide (CuO) has been studied immensely in recent years due to its typical p-type nature, narrow band gap (1.2 eV), low cost, high specific capacitances, favorable pseudo-capacitive characteristics and non-toxicity [12-14]. These appealing properties make it suitable in different fields of research, such as, electrical, gas sensing, optical and heterogeneous catalysis, photovoltaic devices, magnetic storage media, field-emission emitters, lithium ion electrode materials, etc [15-21]. The CuO nanostructures based biosensors can sense glucose non-enzymatically with better sensing performance than many other metal oxides. The reason for this sensing property can be assigned to its better electrochemical activity and its ability to enhance electron transfer reactions [22]. Until now, variable CuO nanostructures like CuO NPs, nanowires, CuO nanorods, flower-shaped CuO have been investigated and explored for glucose

detection with considerable gains [23-25]. However, attaching and maintaining the structure/activity of nano-catalyst on a solid support (electrode) in a fast and reproducible manner, prompts a point to explore. Thus, deposition of CuO nanostructures on the conductive electrode for electrochemical sensor remains intact to the technical issues. Nozzle-jet printing is a successful and an effective manufacturing technique, capable to fabricate/deposit semiconductors and conductive structures on different substrates for sensing applications [26, 27]. Moreover, this printing technique can reduce the cost of fabrication during sensor development. However, the main problem for this printing technology is ink formulation. The ink printing and jetting performance through nozzle on different substrates is directly governed by rheological parameters, such as viscosity and surface tension [28, 29]. Ethylene glycol, poly (vinyl alcohol), glycerol and sodium carboxymethyl cellulose have been utilized to maintain the viscosity of ink [30, 31]. Ethylene glycol and water are the most widely used dispersing solvents for CuO NPs dispersion [32]. Even the CuO NPs remain dispersed in water for days by simply employing an optimized combination of stirring and sonication without using any additive or stabilizer [32, 33]. Thus, we formulated water-based CuO NP ink and short chain alkyl amine based Ag ink for sensor fabrication.

In this study, for the first time, we report fully nozzle-jet printed CuO NPs/Ag/PET non-enzymatic glucose biosensor. The electrochemical performance of the non-enzymatic biosensor towards glucose was studied in alkaline media. The sensing performance was found to be better than those from other CuO morphological nanostructures integrated on the different conductive electrodes such as, gold or platinum by using cross-linkers or sol-gel process. The nozzle-jet printed CuO NPs on Ag printed PET substrate offers excellent attachment due to high porosity

and large surface area of CuO NPs. Moreover, the nozzle-jet printed CuO NPs/Ag/PET electrodes were applied to can measure glucose concentrations in blood and serum samples.

## 2. Experimental details

### *2.1. Reagents*

D-(+)-glucose (≥99.5%), copper acetate dihydrate [$Cu(CH_3COO)_2.2H_2O$], sodium hydroxide (NaOH, 96% purity), acetic acid (≥99.7%), ethylene glycol (99.8%), ascorbic acid (AA, ≥99%), lactose (≥99%), mannose (≥99%), dopamine (DA, ≥98%), L-cysteine (97%), uric acid (UA, ≥99%) and human serum sample (H4522) were purchased from Sigma-Aldrich. Isopropanol (>99.5%), ethanol (>94.5%), and methanol (>99.5%) were purchased from Daejung, Korea. All the chemicals were used as received without further purification. Ultrapure water purified with micro pure HIQ with resistivity of ~18 MΩ cm was exclusively utilized in all aqueous solutions and rinsing procedure.

### *2.2. Synthesis of CuO NPs*

In a typical synthesis procedure, 100 mL aqueous solution of 0.02 M copper acetate was thoroughly mixed with 0.50 mL acetic acid followed by slow heating in a three-necked refluxing flask under stirring. 0.50 g of NaOH was added, as the temperature of solution reached to 90 °C, which formed black color solution (pH = 5-6) specifying the formation of CuO NPs. In this reaction process, NaOH provides basic media and acetic acid prevents precipitate formation of uniformly grown CuO NPs. After 10-15 min refluxing, black-colored colloidal solution was centrifuged at 3000 rpm for 2 min and washed several times with deionized water and ethanol.

### *2.3. Ink-formulation and nozzle-jet printing*

Ag ink formulation and printing properties were discussed in detail in our previous studies [34, 35]. In brief, to formulate CuO NPs ink, first, we prepared a solution of mixed solvents (i.e. 1 mL methanol, 5 mL isopropyl alcohol, 2 mL ethylene glycol, 10 mL deionized water, and 2 mL ethanol) in the ratio of 1:5:2:10:2 volume %. Then, prepared mixture was sonicated for 20 min and stirred at 1000 rpm for 24h. In the next step, as-synthesized CuO NPs were dispersed in the above prepared solution and concentration of CuO NPs was adjusted to 60 weight %.

To fabricate non-enzymatic biosensor (Fig. 1), first, Ag was printed by nozzle-jet printer on the cleaned PET substrate using Ag ink. Then, CuO NPs ink was printed over Ag/PET substrates using same printing technique. Uniform and straight lines were achieved by maintaining various parameters such as moving speed of nozzle (~4000 mm/s), nozzle pressure (~40 kPa), nozzle tip diameter (100 μm), stage-plate temperature (80 $^{0}$C for Ag ink and 110 $^{0}$C for CuO NPs ink printing), and height between nozzle tip and substrate (12 mm). The as-printed CuO films were post-annealed at 80 $^{0}$C in an oven for 3h before characterizations and sensing measurements.

### *2.4. Apparatus and electrochemical measurements*

The structural investigation of as-synthesized CuO NPs was carried out by transmission electron microscopy (TEM) equipped with digital charge-coupled device (JEOL-JEM-2010 equipped with CCD camera). Crystallinity of the CuO NPs was examined by X-ray diffraction (XRD, Rigaku) with Cu-Kα radiation (λ = 1.54178 Å) in the range of 30-70° at 40 kV. Single crystallinity and chemistry of as-grown CuO NPs were examined with selected area electron diffraction (SAED) and elemental mapping energy-dispersive X-ray spectroscopy (EDS), respectively. Optical characterization of CuO NPs was carried out by UV-Visible spectroscopy.

The morphological characterization of printed CuO NPs was analyzed by using field emission scanning electron microscopy (FESEM, Hitachi S4700), atomic force microscopy (AFM). All printing experiments were performed using a commercial nozzle-jet printer (System Engineering Solution (SES, Korea). The cyclic voltammetry (CV) and amperometric measurements were carried out using an electrochemical analyzer connected to a personal computer. All experiments were carried out using a conventional three-electrode system with the CuO NPs/Ag/PET as the working electrode, a platinum (Pt) wire as the counter electrode, and Ag/AgCl with saturated KCl solution as the reference electrode. All the potentials in this work were measured with respect to Ag/AgCl reference electrode and the electrochemical measurements were carried out at room temperature in 0.10 M NaOH. Each CV was performed in a solution of 15 mL volume between -0.2 and +0.80 V (*vs.* Ag/AgCl). In steady state amperometric experiments, the potential was set at +0.60 V (*vs.* Ag/AgCl) while stirring the solution using magnetic bar.

## 3. Results and discussion

### *3.1. Structural and optical characterization of CuO NPs*

Fig. 2 shows the low resolution TEM image (a), and HR-TEM image (b) of CuO NPs. As it can be seen from the images, CuO NPs are nearly spherical in shape with relatively average diameter of ~11-20 nm. From HR-TEM image, the distance between two neighboring lattice fringes was measured as 0.27 nm, which corresponds to the [110] lattice fringe of the monoclinic structure of CuO. Its corresponding SAED pattern (FFT image, inset of c) and elemental mapping (d) confirms the single crystallinity of as-grown CuO NPs. The XRD pattern (Fig. 2e) shows characteristic diffraction peaks of only monoclinic CuO phase [36, 37]. Besides the characteristic CuO peaks, there were no other peaks corresponding to impurities or other crystal

phases such as $Cu_2O$ and $Cu(OH)_2$, which confirms that the as-grown CuO NPs are of high purity. From UV-visible spectrum, the peak at 300 nm is observed due to surface plasmon absorption of metal oxide (Fig. 2f). The surface plasmon absorption effect is due to the collective oscillation of the free conduction band electrons which is excited by the incident electromagnetic radiation in the metal oxide nanoparticles [38]. This type of resonance occurs when the incident light with certain wavelength far exceeds the particle diameter. Surface plasmon absorption band with a maximum at 300 nm indicates the formation of CuO NPs.

### *3.2. Characterization of Ag and CuO NPs inks printed on PET*

The as-formulated inks were printed sequentially on PET substrate. The optical image of printed non-enzymatic electrode is shown in the Fig. 3a (inset). The fully nozzle-jet printed CuO NPs yielded CuO NPs/Ag/PET electrodes which also showed better adhesion between CuO NPs and Ag/PET electrode and had working area of 2×5 $mm^2$. During printing, proper viscosity of ink is important for jetting and good wettability of ink on substrate to make uniform film morphology. Fig. 3(a, b) shows FESEM image of overprinted CuO NPs on Ag printed lines. It can be seen clearly that as-printed CuO line possessed uniform and densely porous morphology. Two dimensional (2D) surface profiler image illustrate height of the overprinted CuO line with thickness of ~1.5 µm (Fig. 3c). The EDS analysis shows that as-printed CuO NPs line exhibited only CuO phase with no impurity or additive left out after annealing in an oven for 3h at 80 $^0$C (Fig. 3d). The printed CuO pattern shows a smooth surface topography without any structural defects with root-mean-square (rms) roughness of 20.4 nm (Fig. 3e, f). Moreover both printed Ag and CuO inks did not show any defects such as bulging or coffee-ring effect while printing or annealing process.

### *3.3. Electrochemical properties of fully printed non-enzymatic electrode and glucose detection*

The fabrication process of Ag/PET and CuO NPs/Ag/PET electrodes were pre-examined by electrochemical impedance spectroscopy (EIS) measurements to study the changes of electrode surface state and charge transfer properties of the electrode (Fig. 4a). For EIS spectrum measurement, an electron transfer probe [$Fe(CN)_6^{3-/4-}$] was used for electrode surface characterization. After each impedance measurement, the Randle equivalent circuit model was used to fit obtained data (inset of Fig. 4a). In this circuit the solution resistance ($R_s$) is in series with charge transfer resistance ($R_{ct}$) and in parallel with double-layer capacitance ($C_{dl}$). The semicircle diameter of the Nyquist plot indicates the charge transfer resistance ($R_{ct}$) which controls the electron transfer kinetics of the redox probe at the electrode surface. The EIS spectrum of Ag/PET electrode (i) shows no semicircle for $R_{ct}$ value which means smooth charge transfer rate due to high conductivity of printed Ag. However, after printing of CuO NPs on Ag/PET electrode (ii), the Nyquist semicircle becomes larger which most probably might be due to the hindrance of electron transfer caused by CuO NPs. Thus, it indicates the successful fabrication of CuO NPs/Ag/PET electrodes by nozzle-jet printing at low temperature.

Moreover, the electrochemical properties of fully printed electrodes (CuO NPs/Ag/PET) were characterized by CV method in 0.1 M NaOH solution between the potentials of -0.2 and +0.8V. Fig. 4b shows the CV curves of Ag printed electrode (Ag/PET, black curve) and fully printed CuO NPs/Ag/PET electrode (red curve) in the absence of glucose, which shows no redox reaction. However, after addition of 2.0 mM glucose (blue curve) fully printed CuO NPs/Ag/PET electrode showed increase in current signal toward the positive end of the potential range. It can be clearly seen that the oxidation process begins in presence of glucose at approximately +0.2V with very broad peak at around +0.60 V. Fig. 4c shows the CVs of fully printed CuO NPs/Ag/PET electrode performed at different scan rates (50-300 mV/s) in the presence of 5 mM

glucose 0.10 M NaOH solution. From the calibrated curve (i.e. anodic peak current *versus* scan rate) shows the linear increase in anodic peak current with increasing scan rate (insets of Fig. 4c), confirming that the glucose oxidation is a surface controlled electrochemical process [39, 40]. A linear regression equation (y = 11.8X + 2694) was obtained from the graph with correction coefficient ($R^2$) of 0.99715. This indicates that nozzle-jet printed CuO NPs/Ag/PET electrode greatly enhances the sensing performance, which is attributed to the porosity, large surface area and enhanced electron transfer properties of printed CuO NPs. First, Marioli and Kuwana, later by Wei *et. al.* suggested the oxidation mechanism of glucose on the modified copper-based electrodes [41, 42]. The oxidation process begins with deprotonation of glucose and subsequently isomerization to its enediol form. The later get adsorbed onto the electrode surface, following oxidation by Cu(II) and Cu(III). The possible reaction could be explained by the following equations [43].

$$CuO + OH^- \rightarrow CuOOH + e^- \quad \text{(i)}$$

$$CuOOH + e^- + \text{glucose} \rightarrow CuO + OH^- + \text{gluconic acid} \quad \text{(ii)}$$

During CV measurement, primarily CuO NPs gets oxidized from Cu(II) to Cu(III). Then, it catalyzes glucose oxidation reaction to liberate gluconolactone which upon further oxidation converts to gluconic acid. Here, it is clear that Cu(II)/Cu(III) redox couple assists the catalysis reaction by CuO in the electrochemical non-enzymatic detection of glucose. Thus, an enhanced catalytic current response on our CuO NPs/Ag/PET electrode in the presence of glucose solution is observed and it further depends upon the glucose concentration.

The amperometric response under different glucose concentration solutions (0.1-17.6 mM) was determined to investigate the performance of fully printed non-enzymatic electrode (CuO NPs/Ag/PET). Fig. 5a shows amperometric response of CuO NPs/Ag/PET printed electrode on the successive addition of glucose into continuously stirred 0.1 M NaOH solution at

a working potential of +0.6V. The printed non-enzymatic electrode exhibits a sensitive amperometric response and an obvious increase in current with successive increase in glucose concentration. From the graph, a clear rapid steady state current increase is evident with increasing addition of glucose i.e. from 0.1 to 17.6 mM. Further, the sensitive non-enzymatic electrode showed a short response time of ~2s. From the calibration plot (Fig. 5b), the sensitivity was calculate to be 1424.2 μA $mM^{-1}$ $cm^{-2}$ in the wide linear range from 0. 1 to 15 mM with high linear relationship between glucose concentration and current response ($R^2 = 0.9989$). Moreover, the low detection limit (LOD) was estimated to be 0.3 μM (based on signal/noise (S/N) ratio of 3) for the nozzle-jet printed non-enzymatic electrode. A comparative study (Table 1) reveals high sensitivity, low detection limit, wide linear range and relatively fast response, which are far better results obtained for our fully nozzle-jet printed biosensor than other sensors fabricated by different methods [44-55]. The high sensitivity and wide linear range of fully nozzle-jet printed sensor are mainly attributed to porous nature of printed CuO NPs (due to fast evaporation of solvents during drying of printed CuO NPs ink) which provides the higher specific surface area and the strong adhesion of the printed material on PET which enables fast and direct conduction of electron resulting in faster response and high sensitivity.

### *3.4. Anti-interference*

The nozzle-jet printed CuO NPs/Ag/PET electrodes were further evaluated for anti-interference test. The anti-interference test is considered to be an effective parameter for electrochemical based sensing of glucose associated with other similar chemically composition biological molecules, as the oxidation potential of glucose may be correlated to the oxidation potential of other interfering species. Therefore, both lower and higher concentration interferants were employed to analyze the selectivity of non-enzymatic electrode by amperometry which in

turn governs its accuracy. Interference test was carried out by successive addition of 1 mM glucose and 0.10 mM of each interfering species i.e. AA, L-cysteine, UA, mannose, lactose, and DA; followed by subsequent addition of 1 mM glucose and 0.5 mM interfering species in 15 mL of 0.1 M NaOH solution at an applied potential of +0.6V (Fig. 5c). The addition of 1 mM glucose resulted in significant and quick current response, whereas the sensing performance was not affected or caused negligible current changes by addition of 0.10 mM and 0.5 mM of each interfering species. From the results obtained, our fully nozzle-jet sensor shows reliable anti-interference property and is also highly suitable for detection of glucose in real samples. Besides, the chloride poisoning of the non-enzymatic electrodes were also checked by introducing chloride poisons (citric acid, sodium citrate, NaCl, and $KH_2PO_4$), which shows no significant effect on sensor response (Fig. 5d). It governs that our fully printed non-enzymatic electrodes are exclusively chloride poisons resistance.

### *3.5. Reproducibility and stability test of nozzle-jet printed non-enzymatic electrodes*

Fig. 6a shows the reproducibility test of five nozzle-jet printed CuO NPs/Ag/PET non-enzymatic electrodes prepared in similar conditions for the detection of 5.0 mM glucose in 0.1 M NaOH solution by CV. The calibrated histogram (Fig. 6b) shows a good relative standard deviation (RSD) of ~2%. The fabricated non-enzymatic electrode was also evaluated for ten times showing better repeatability with a RSD of 2.5%. Additionally the long-term stability of the printed CuO NPs/Ag/PET non-enzymatic electrode was regularly evaluated for the detection of 5.0 mM glucose in 0.1 M NaOH solution by CV for eight weeks while storing under ambient conditions (Fig. 6c). The corresponding histogram shows that the calibrated CV responses explicit excellent stability as the decrease in sensitivity of the non-enzymatic electrode was only around ~5% even after eight weeks of storage (Fig. 6d). In general, the present fully printed

glucose sensing non-enzymatic electrode with excellent reproducibility and stability can be considered to be quite reliable for glucose determination.

### *3.6. Real sample analysis*

To verify the workability, nozzle-jet printed electrodes were applied for the determination of glucose in human blood and serum sample. For both sample, three nozzle-jet printed electrodes were used for the determination of glucose concentration. During CV measurement, CuO NPs/Ag/PET as working, Ag/AgCl as reference and Pt as counter electrode were immersed in 15 mL of 0.1 M NaOH solution containing human blood and serum sample (Fig. 7a and 7b). The obtained current response during CV measurement in human blood and serum sample are compared in histogram (Fig. 7c). From histogram, it can be seen that the glucose concentration in human blood sample is comparable to that of serum sample, which confirms the selectivity of the sensor in the presence of other biomolecules and protein fragments [56-58]. Also, the measured glucose concentration (4.75±0.17 mM) in serum sample using our nozzle-jet printed electrode is in good agreement with the pre-analytically determined known concentration (4.88 mM) of glucose in serum sample.

## 4. Conclusions

In summary, we have successfully nozzle-jet printed non-enzymatic glucose biosensor (CuO NPs/Ag/PET) electrodes by employing CuO NPs ink as a sensing material, Ag ink as conductive electrode, and PET as a flexible substrate. During electrochemical characterizations, the fully printed non-enzymatic biosensor exhibited a high sensitivity (1424.2 μA $mM^{-1}cm^{-2}$), wide linear range (0.1 to 15 mM), low detection limit (0.3 μM), fast response time (~2s), excellent long term stability, high reproducibility, good selectivity and applicability in human

blood and serum samples. Additionally, nozzle-jet printing method can easily be employed for the fabrication of electrodes in large scale. Hence, nozzle-jet printing technique can promote an efficient strategy for the development of low-cost and environmental friendly, highly stable and better performing sensing electrodes for various applications.

**Acknowledgements**

This work was supported by the National Leading Research Laboratory program through the National Research Foundation (NRF) (NRF-2016R1A2B2016665) of Korea funded by the Ministry of Science, ICT & Future Planning. Authors also thank KBSI, Jeonju branch for SEM analysis and Mr. Jong-Gyun Kang, Center for University Research Facility (CURF) for taking good quality TEM images.

**References**

[1] N. Mitro, P.A. Mak, L. Vargas, C. Godio, E. Hampton, V. Molteni, A. Kreusch, E. Saez, The nuclear receptor LXR is a glucose sensor, Nature 445 (2007) 219-223.

[2] Y. Huang, X. Dong, Y. Shi, C.M. Li, L.-J. Li and P. Chen, Nanoelectronic biosensors based on CVD grown graphene, Nanoscale 2 (2010) 1485-1488.

[3] J. Wang. Electrochemical Glucose Biosensors, Chem. Rev. 108 (2008) 814-825.

[4] J. Shi, H. Zhang, A. Snyder, M.-X. Wang, J. Xie, D.M. Porterfield, L.A. Stanciu, An aqueous media based approach for the preparation of a biosensor platform composed of graphene oxide and Pt-black, Biosens. Bioelectron. 38 (2012) 314-320.

[5] Y.-B. Hahn, R. Ahmad, N. Tripathy, Chemical and biological sensors based on metal oxide nanostructures, Chem. Commun. 48 (2012) 10369-10385.

[6] Y. Song, K. Qu, C. Zhao, J. Ren, X. Qu, Graphene Oxide: Intrinsic Peroxidase Catalytic Activity and Its Application to Glucose Detection, Adv. Mater. 22 (2010) 2206-2210.

[7] E.S. Forzani, H. Zhang, L.A. Nagahara, I. Amlani, R. Tsui, N. Tao, a conducting polymer nanojunction sensor for glucose detection, Nano Lett. 4 (2004) 1785-1788.

[8] X.-C. Dong, H. Xu, X.-W. Wang, Y.-X. Huang, B. C.-P. Mary, H. Zhang, L.-H. Wang, W. Huang, P. Chen, 3d graphene-cobalt oxide electrode for high-performance supercapacitor and enzymeless glucose detection, ACS Nano 6 (2012) 3206-3213.

[9] A.-B. Zahra, N.-E. Alireza, A novel non-enzymatic glucose sensor based on the modification of carbon paste electrode with CuO nanoflower: Designing the experiments by response surface methodology (RSM), J. Colloid Interface Sci. 504 (2017) 186-196.

[10] C. Li, Y. Liu, L. Li, Z. Du, S. Xu, M. Zhang, X. Yin, T. Wang, A novel amperometric biosensor based on NiO hollow nanospheres for biosensing glucose, Talanta 77 (2008) 455-459.

[11] M. Shamsipur, M. Najafi, M.-R. M. Hosseini. Highly improved electrooxidation of glucose at a nickel(II) oxide/multi-walled carbon nanotube modified glassy carbon electrode, Bioelectrochemistry 77 (2010) 120-124.

[12] H. Huang, Y. Liu, J. Wang, M. Gao, X. Peng, Z. Ye, Self-assembly of mesoporous CuO nanosheets-CNT 3D network composites for lithium-ion batteries, Nanoscale 5 (2013) 1785-1788.

[13] Z. Guo, M.-L. Seol, M.-S. Kim, J.-H. Ahn, Y.-K. Choi, J.-H. Liu, X.-J. Huang, Hollow CuO nanospheres uniformly anchored on porous Si nanowires: Preparation and their potential use as electrochemical sensors, Nanoscale 4 (2012) 7525-7531.

[14] M.A. Dar, Q. Ahsanulhaq, Y.S. Kim, J.M. Sohn, W.B. Kim, H.S. Shin, Versatile synthesis of rectangular shaped nanobat-like CuO nanostructures by hydrothermal method; structural properties and growth mechanism, Appl. Surf. Sci. 255 (2009) 6279-6284.

[15] J. Kim, W. Kim, K. Yong, CuO/ZnO heterostructured nanorods: photochemical synthesis and the mechanism of $H_2S$ gas sensing, J. Phys. Chem. C 116 (2012) 15682-15691.

[16] D. Cao, C. Wang, F. Zheng, W. Dong, L. Fang, M. Shen, high-efficiency ferroelectric-film solar cells with an n-type $cu_2o$ cathode buffer layer, Nano Lett. 12 (2012) 2803-2809.

[17] Y.W. Zhu, T. Yu, F.C. Cheong, X.J. Xu, C.T. Lim, V.B.C. Tan, J.T. L. Thong, C.H. Sow, Large-scale synthesis and field emission properties of vertically oriented CuO nanowire films, Nanotechnology 16 (2005) 88-92.

[18] X. Gou, G. Wang, J. Yang, J. Park, D. Wexler, Chemical synthesis, characterisation and gas sensing performance of copper oxide nanoribbons, J. Mater. Chem. 18 (2008) 965-969.

[19] M.A. Dar, Y.S. Kim, W.B. Kim, J.M. Sohn, H.S. Shin, Structural and magnetic properties of CuO nanoneedles synthesized by hydrothermal method. Appl. Surf. Sci. 254 (2008) 7477-7481.

[20] E.-H. Javad, N.-E. Alireza, Increased photocatalytic activity of Zn(II)/Cu(II) oxides and sulfides by coupling and supporting them onto clinoptilolite nanoparticles in the degradation of benzophenone aqueous solution, J. Hazard. Mater. 316 (2016) 194-203.

[21] S. Arezoo, N.-E. Alireza, Enhanced photocatalytic activity of supported CuO-ZnO semiconductors towards the photodegradation of mefenamic acid aqueous solution as a semi real sample, J. Mol. Catal. A: Chem. 411 (2016) 222-229.

[22] S.K. Meher, G.R. Rao, Archetypal sandwich-structured CuO for high performance non-enzymatic sensing of glucose. Nanoscale 2013, 5, 2089-2099.

[23] J. Dong, L. Ren, Y. Zhang, X. Cui, P. Hu, J. Xua, Direct electrodeposition of cable-like CuO@Cu nanowires array for non-enzymatic sensing, Talanta 132 (2015) 719-726.

[24] C. Chen, S.H. Lee, M. Cho, Y. Lee, Core-shell CuO@$TiO_2$ nanorods as a highly stable anode material for lithium-ion batteries, Mater. Lett. 140 (2014) 111-114.

[25] M.-J. Song, S.-K. Lee, J.-H. Kim, D.-S. Lim, Non-enzymatic glucose sensor based on Cu electrode modified with CuO nanoflowers, J. Electrochem. Soc. 160 (2013) B43-B46.

[26] Y. Wang, M. Y. Khan, S.-K. Lee, Y.-K. Park, Y.-B. Hahn, Parametric study of nozzle-jet printing for directly drawn ZnO field-effect transistors. Sci. Adv. Mater. 7 (2015) 1-8.

[27] K.S. Bhat, R. Ahmad, J.-Y. Yoo, Y.-B. Hahn, Nozzle-jet printed flexible field-effect transistor biosensor for high performance glucose detection, J. Colloid Interface Sci. 506 (2017) 188-196.

[28] Y.H. Yun, J.D. Kim, B.K. Lee, B. Yoo, J.-H. Lee, Y. W. Cho, Construction of micro-patterned polymer structures by piezoelectric inkjet printing, Polym. Plast. Technol. Eng. 48 (2009) 1318-1323.

[29] Y.H. Yun, J.D. Kim, B.K. Lee, Y.W. Cho, H.Y. Lee, Polymer inkjet printing: construction of three-dimensional structures at micro-scale by repeated lamination, Macromol. Res. 17 (2009) 197-202.

[30] S.D. Risio, N.Yan, Piezoelectric ink-jet printing of horseradish peroxidase: Effect of ink viscosity modifiers on activity, Macromol. Rapid Commun. 28 (2007) 1934-1940.

[31] L. Setti, A. Fraleoni-Morgera, B. Ballarin, A. Filippini, D. Frascaro, C. Piana, An amperometric glucose biosensor prototype fabricated by thermal inkjet printing, Biosens. Bioelectron. 20 (2005) 2019-2026.

[32] G. Tertsinidou, M.J. Assael, W.A. Wakeham, The apparent thermal conductivity of liquids containing solid particles of nanometer dimensions: A critique. Int. J. Thermophys. 36 (2015) 1367-1395.

[33] R. Karthik, R. H. Nagarajan, B. Raja, P. Damodharan, Thermal conductivity of CuO-DI water nanofluids using 3-ω measurement technique in a suspended micro-wire, Exp. Thermal Fluid Sci. 40 (2012) 1-9.

[34] K.S. Bhat, R. Ahmad, Y. Wang, Y.-B. Hahn, Low-temperature sintering of highly conductive silver ink for flexible electronics, J. Mater. Chem. C 4 (2016) 8522-8527.

[35] M. Vaseem, A.-R. Hong, R.-T. Kim, Y.-B. Hahn. Copper oxide quantum dot ink for inkjet-driven digitally controlled high mobility field effect transistors, J. Mater. Chem. C 1 (2013) 2112-2120.

[36] M. Vaseem, A. Umar, Y.-B. Hahn, D.H. Kim, K.S. Lee, J.S. Jang, J.S. Lee, Flower-shaped CuO nanostructures: Structural, photocatalytic and XANES studies, Catal. Commun. 10 (2008) 11-16.

[37] N.-E. Alireza, K.-S. Maryam, Decolorization of a binary AZO dyes mixture using CuO incorporated nanozeolite-X as a heterogeneous catalyst and solar irradiation. Chem. Eng. J. 228 (2013) 631-641.

[38] N.-E. Alireza, S. Zahra, Solar photocatalytic degradation of o-phenylenediamine by heterogeneous CuO/X zeolite catalyst, Desalination 280 (2011) 281-287.

[39] N. Azin, N.-E. Alireza, A novel and sensitive carbon paste electrode with clinoptilolite nanoparticles containing hexadecyltrimethyl ammonium surfactant and dithizone for the voltammetric determination of Sn(II), J. Colloid Interface Sci. 501 (2017) 321-329.

[40] H.S.-M. Mohammad, N.-E. Alireza, Modification of carbon paste electrode with Ni-clinoptilolite nanoparticles for electrocatalytic oxidation of methanol, Electrochim. Acta 147 (2014) 572-581.

[41] J.M. Mariolia, T. Kuwana, Electrochemical characterization of carbohydrate oxidation at copper electrodes, Electrochim. Acta 37 (1992) 1187-1197.

[42] H. Wei, J.-J. Sun, L. Guo, X. Li, G.-N. Chen. Highly enhanced electrocatalytic oxidation of glucose and shikimic acid at a disposable electrically heated oxide covered copper electrode. Chem. Commun. 20 (2009) 2842-2844.

[43] S. Sun, X. Zhang, Y. Sun, S. Yang, X. Song, Z. Yang, Hierarchical CuO nanoflowers: water-required synthesis and their application in a nonenzymatic glucose biosensor, Phys. Chem. Chem. Phys. 15 (2013) 10904-10913.

[44] A. Molazemhosseini, L. Magagnin, P. Vena, C.-C. Liu, Single-use nonenzymatic glucose biosensor based on CuO nanoparticles ink printed on thin film gold electrode by micro-plotter technology, J. Electroanal. Chem. 789 (2017) 50-57.

[45] L.-C. Jiang, W.-D. Zhang, A highly sensitive nonenzymatic glucose sensor based on CuO nanoparticles-modified carbon nanotube electrode, Biosens. Bioelectron. 25 (2010) 1402-1407.

[46] E. Reitz, W. Jia, M. Gentile, Y. Wang, Y. Lei, CuO nanospheres based nonenzymatic glucose sensor, Electroanalysis 20 (2008) 2482-2486.

[47] R. Ahmad, M. Vaseem, N. Tripathy, Y.B. Hahn, Wide linear-range detecting nonenzymatic glucose biosensor based on CuO nanoparticles inkjet-printed on electrodes, Anal. Chem. 85 (2013) 10448-10454.

[48] M. Saraf, K. Natarajan, S.M. Mobin, Non-enzymatic amperometric sensing of glucose by employing sucrose templated microspheres of copper oxide (CuO), Dalton Trans. 45 (2016) 5833-5840.

[49] X. Wang, C. Hu, H. Liu, G. Du, X. He, Y. Xi, Synthesis of CuO nanostructures and their application for nonenzymatic glucose sensing, Sens. Actuators B Chem. 144 (2010) 220-225.

[50] R. Ahmad, N. Tripathy, Y.-B. Hahn, A. Umar, A.A. Ibrahim, S.H. Kim, A robust enzymeless glucose sensor based on CuO nanoseed modified electrodes, Dalton Trans. 44 (2015) 12488-12492.

[51] G. Liu, B. Zheng, Y. Jiang, Y. Cai, J. Du, H. Yuan, D. Xiao, Improvement of sensitive CuO NFs-ITO nonenzymatic glucose sensor based on in situ electrospun fiber, Talanta 101 (2012) 24-31.

[52] S.K. Meher, G.R. Rao, Archetypal sandwich-structured CuO for high performance non-enzymatic sensing of glucose, Nanoscale 5 (2013) 2089-2099.

[53] N.Q. Dung, D. Patil, H. Jung, D. Kim, A high-performance nonenzymatic glucose sensor made of CuO-SWCNT nanocomposites, Biosens. Bioelectron. 42 (2013) 280-286.

[54] C. Li, H. Yamahara, Y. Lee, H. Tabata, J.-J. Delaunay, Nanoporous CuO layer modified Cu electrode for high performance enzymatic and non-enzymatic glucose sensing, Nanotechnology 26 (2015) 305503.

[55] W. Wang, L. Zhang, S. Tong, X. Li, W. Song, Three-dimensional network films of electrospun copper oxide nanofibers for glucose determination, Biosens. Bioelectron. 25 (2009) 708-714.

[56] R. Ahmad, N. Tripathy, Y.-B. Hahn, High-performance cholesterol sensor based on the solution-gated field effect transistor fabricated with ZnO nanorods, Biosens. Bioelectron. 45 (2013) 281-286.

[57] R. Ahmad, N. Tripathy, M.-S. Ahn, K.S. Bhat, T. Mahmoudi, Y. Wang, J.-Y. Yoo, D.-W. Kwon, H.-Y. Yang, Y.-B. Hahn, Highly efficient non-enzymatic glucose sensor based on CuO modified vertically-grown ZnO nanorods on electrode, Sci. Rep. 7 (2017) 5715.

[58] D.-U.-J. Jung, R. Ahmad, Y.-B. Hahn, Nonenzymatic flexible field-effect transistor based glucose sensor fabricated using NiO quantum dots modified ZnO nanorods, J. Colloid Interface Sci. 512 (2018) 21-28.

**Table 1.** Comparison of our nozzle-jet printed non-enzymatic biosensor with previous reports.

| Electrode | Method | Response (s) | Linear range (mM) | Detection limit (µm) | Sensitivity ($\mu A\ mM^{-1}\ cm^{-2}$) | Ref. |
|---|---|---|---|---|---|---|
| CuO NPs/Au/PET | Micro-plotter technology | <5 | 0.1-6.5 | 0.5 | 2419.8 | [37] |
| CuO-MWCNT/TA foil | Sputter | <2 | 0.0004-1.2 | 0.2 | 2596 | [38] |
| CuO nanospheres/GCE | Drop cast | - | 0-2.55 | 1 | 404.53 | [39] |
| CuO NPs/Ag/Si | Inkjet printing | <2 | 0.05-18.45 | 0.5 | 2762.5 | [40] |
| CuO microspheres/SPE | Drop cast | <5 | 2-9 | 20.6 | 26.59 | [41] |
| Flower-shaped CuO/graphite | Solution spray | <15 | - | 4 | 709.52 | [42] |
| CuO nanoseeds/Au/glass | Drop cast | 2 | 0.1-13.3 | 50 | 1101 | [43] |
| CuO NFs/ITO | Electrospinning | - | 0.0002-1.3 | 0.04 | 873 | [44] |
| Sandwich structured CuO/GCE | Drop cast | 0.7 | 0-3.2 | 1 | 5342.8 | [45] |
| CuO-SWCNT/ITO | Co-arc-discharge method and sputtering | <2 | 0.00005-1.8 | 0.05 | 1610 | [46] |
| Nanoporous CuO/Cu | Solution process | 2 | 0.1-2.04 | 2 | 1066 | [47] |
| CuO NFs/GCE | Electrospinning | 1 | 0.006-2.5 | 0.8 | 431.3 | [48] |
| CuO NPs/Ag/PET | Nozzle-jet printing | ~2 | 0.1-15 | 0.3 | 1424.2 | This work |

**Figure captions:**

**Fig. 1.** Schematic illustration of non-enzymatic (CuO NPs/Ag/PET) electrode fabrication process using nozzle-jet printing technique for electrochemical glucose biosensor application.

**Fig. 2.** Bright-field TEM image (a), HR-TEM image (b), corresponding SAED pattern (c), elemental mapping (d), typical XRD and UV-visible spectrum of CuO NPs (f). Inset c shows the FFT image.

**Fig. 3.** FESEM image CuO NPs printed line on Ag line (a, b), 2D surface profiler (c), EDX spectrum (d), and AFM analysis (e, f) of the nozzle-jet printed CuO line. Inset a and b show the optical image of non-enzymatic electrode and FESEM of CuO NPs, respectively.

**Fig. 4.** The Nyquist curves of the EIS spectrum of Ag line printed on PET (curve i) and CuO NPs/Ag/PET electrodes (curve ii) in 0.1 M KCl containing 5.0 mM $K_4Fe(CN)_6$ (a); CV graphs of Ag/PET electrode without (black curve), CuO NPs/Ag/PET electrode without (red curve) and with (red curve) 2.0 mM glucose at the scan rate of 100 mV/s (b); CV graphs at different scan rates in 5.0 mM glucose in 0.1 M NaOH (c). Error bars in c indicate standard deviations of three measurements.

**Fig. 5.** Amperometric steady-state current-time responses of glucose at the CuO NPs/Ag/PET electrode in 0.10 M NaOH at +0.6V (a); Calibration curve (current *vs.* concentration) (b); interference test of the CuO NPs/Ag/PET electrode after successive addition of 1.0 mM glucose, low (0.10 mM) and high (0.5 mM) concentration of each interfering species (c); Chloride poisoning test of the sensor by subsequent addition of 1.0 mM glucose and 0.10 mM of each chlorides (citric acid, sodium citrate, NaCl, and $KH_2PO_4$) in 0.1 M NaOH at an applied potential of +0.6V (*vs.* Ag/AgCl) (d). Error bars in b indicate standard deviations of three measurements.

**Fig. 6.** CV response of five CuO NPs/Ag/PET electrodes prepared in similar conditions for the detection of 5.0 mM glucose in 0.1 M NaOH solution at the scan rate of 100 mV/s (a) and the calibrated histogram showing current response (b); CV response of CuO NPs/Ag/PET electrodes for the detection of 5.0 mM glucose in 0.1 M NaOH solution (c) at the scan rate of 100 mV/s for eight weeks and calibrated histogram showing current response. Error bars in b and d indicate standard deviations of three measurements.

**Fig. 7.** CV response of CuO NPs/Ag/PET electrodes prepared in similar conditions for the detection of glucose in human blood (a) and serum samples (b) in 0.1 M NaOH solution at the scan rate of 100 mV/s, and calibrated histogram showing current response (c). Error bars in c indicate standard deviations of three measurements.

**Figures:**

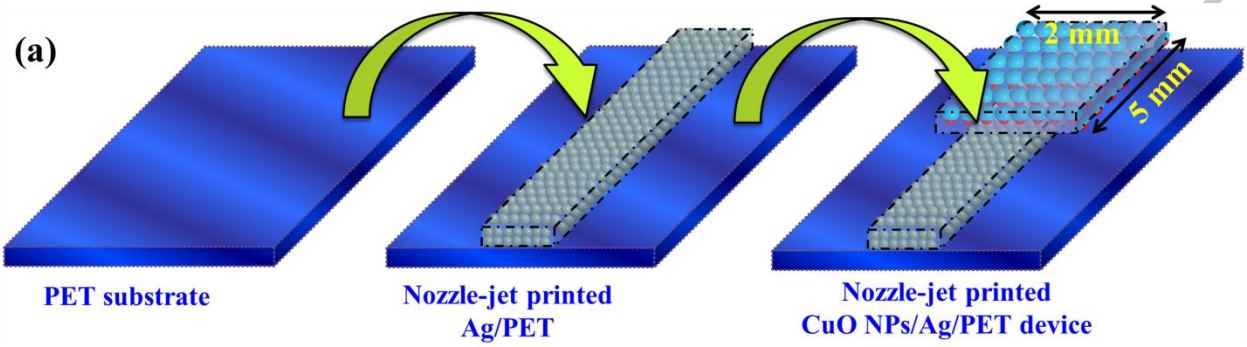


**Fig. 1/7**

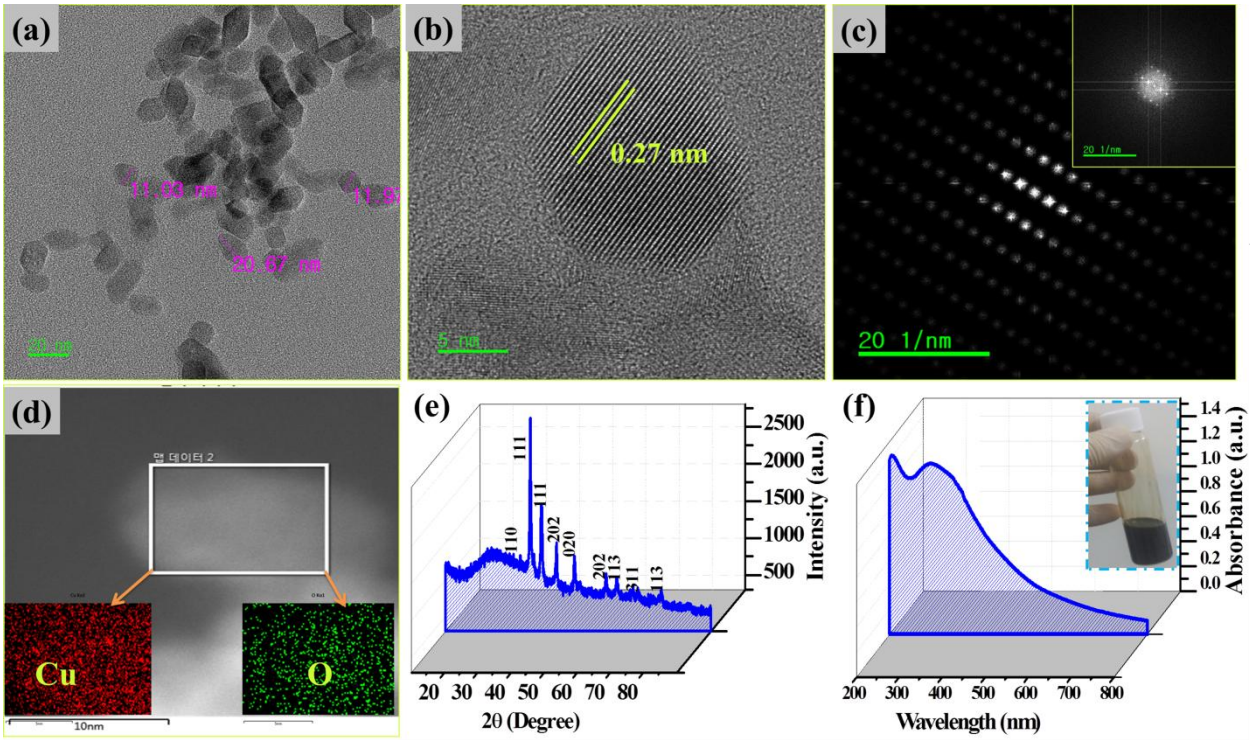


**Fig. 2/7**

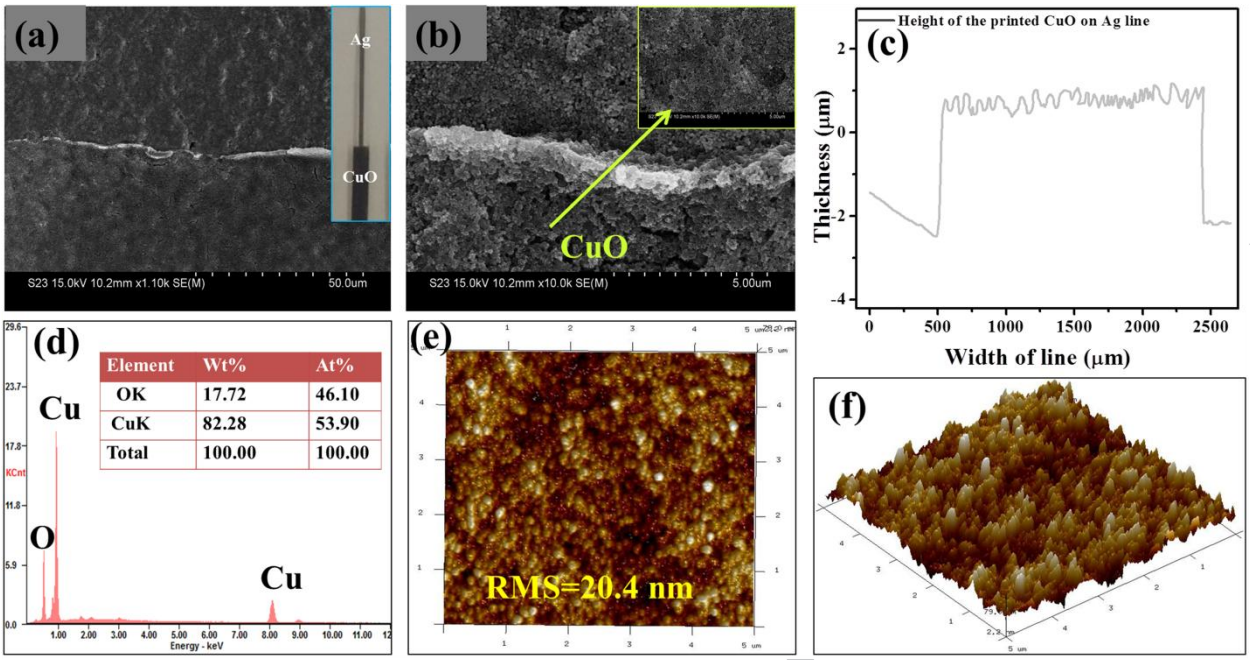


**Fig. 3/7**

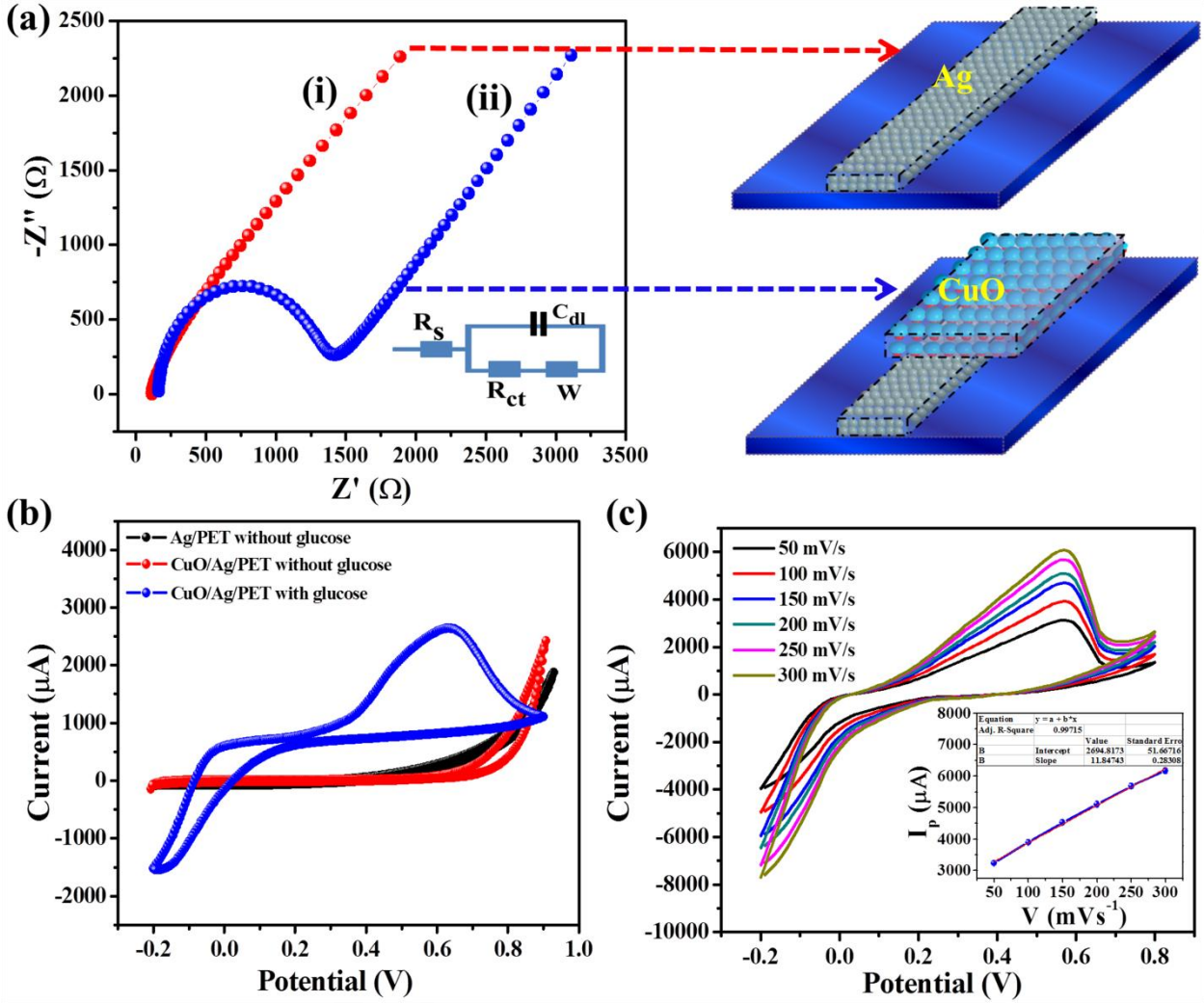
(a)
-Z'' (Ω)
Z' (Ω)
(i)
(ii)
R_S
C_dl
R_ct
W
Ag
CuO
(b)
Ag/PET without glucose
CuO/Ag/PET without glucose
CuO/Ag/PET with glucose
Current (μA)
Potential (V)
(c)
50 mV/s
100 mV/s
150 mV/s
200 mV/s
250 mV/s
300 mV/s
Current (μA)
Potential (V)
I_p (μA)
V (mVs^-1)

**Fig. 4/7**

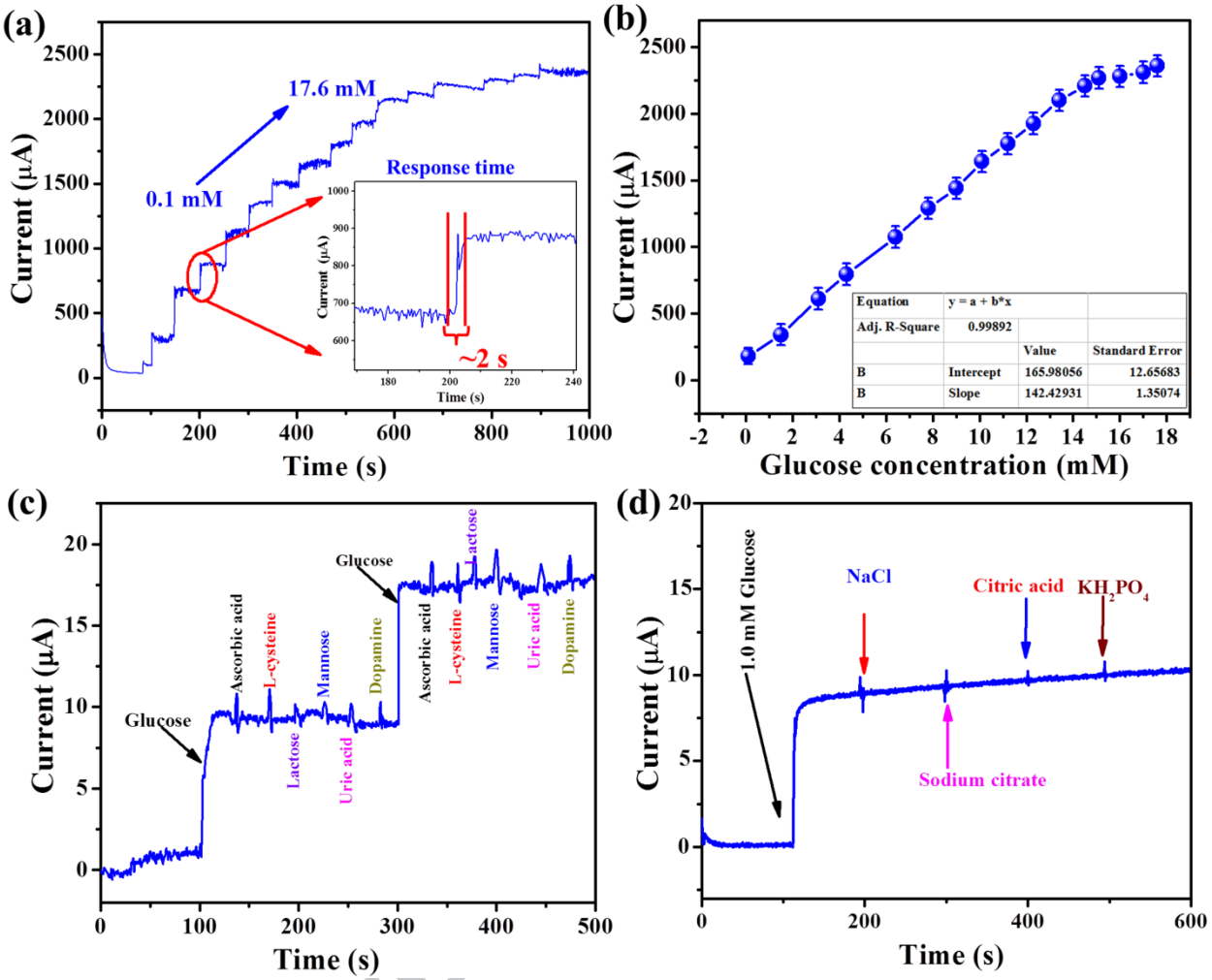


**Fig. 5/7**

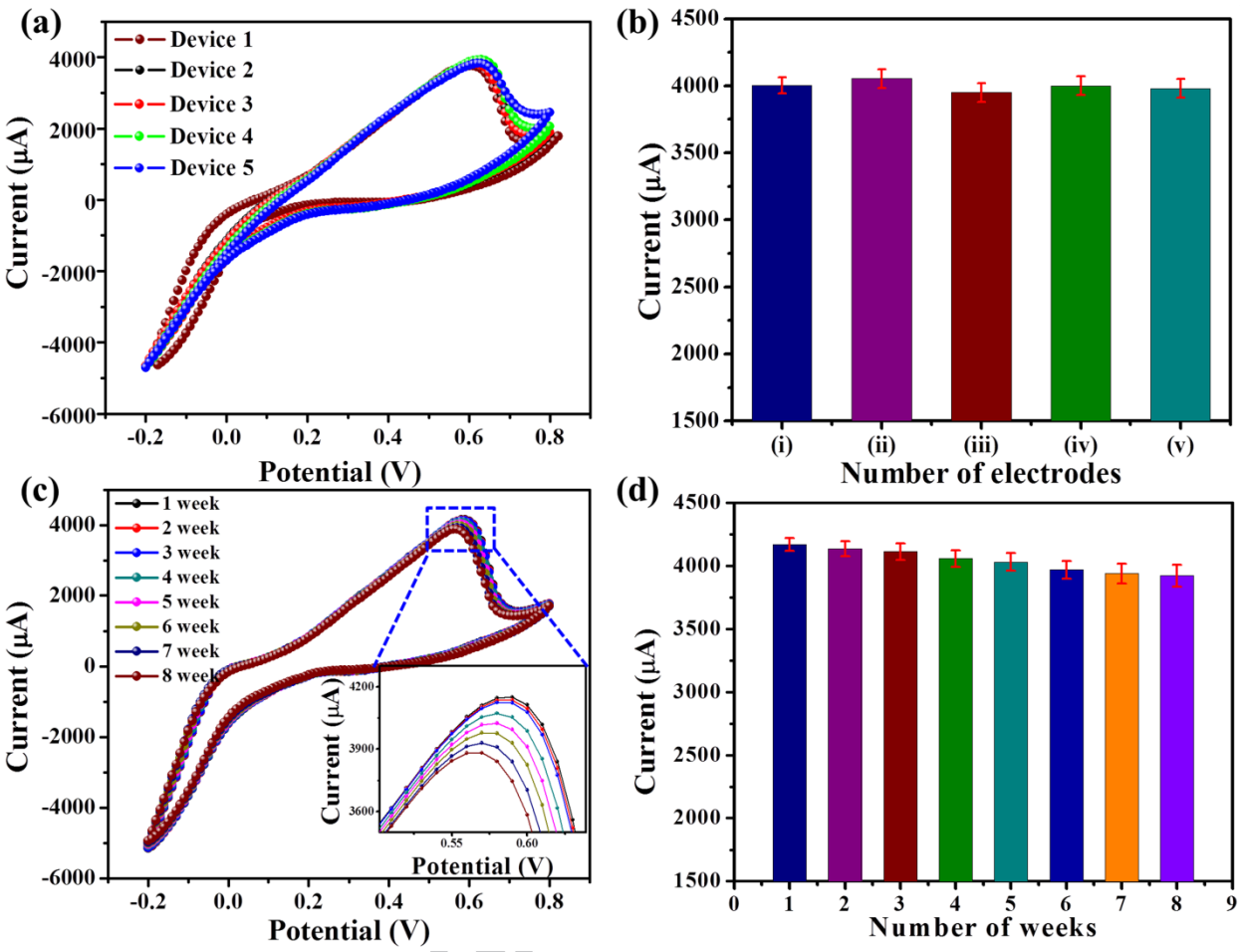


Fig. 6/7

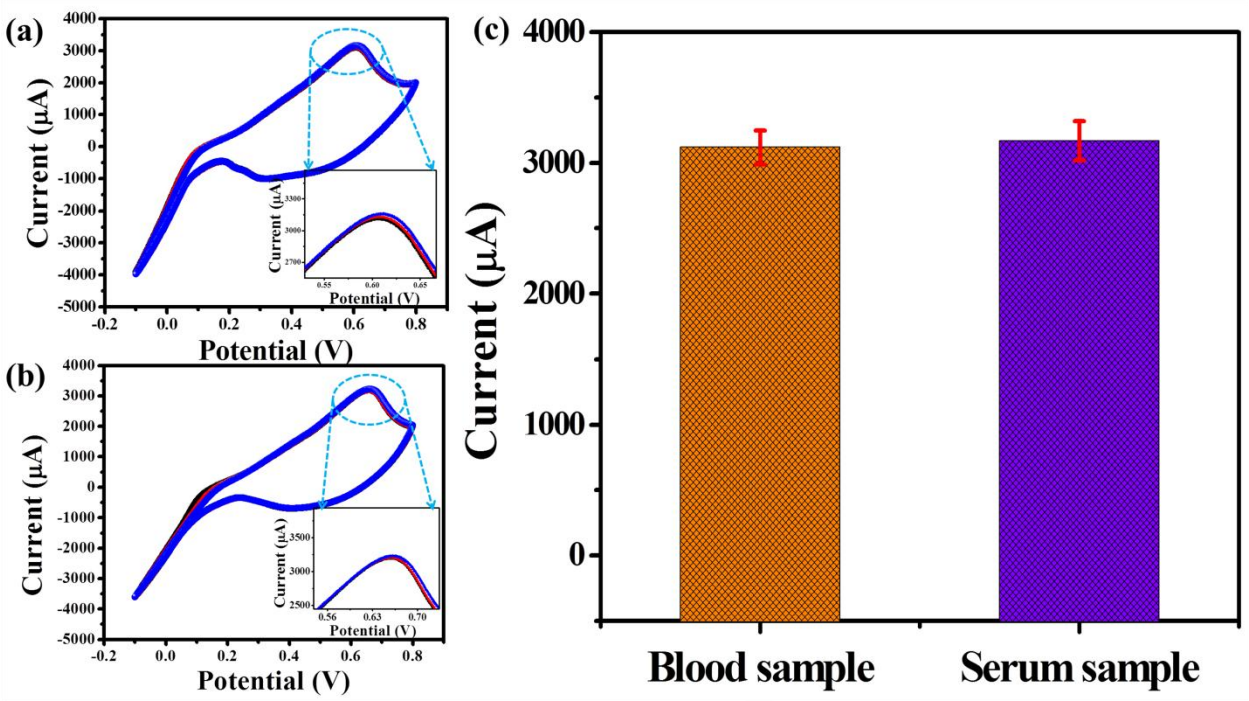


Fig. 7/7

**Graphical abstract**